Transportation Geotechnics 26 (2021) 100419

Contents lists available at ScienceDirect

Transportation Geotechnics

journal homepage: www.elsevier.com/locate/trgeo

Freeze-thaw depth prediction with constrained optimization for spring load restriction

Ting Bao[a,*,1], Behnam Azmoon[b], Zhen (Leo) Liu[c,*]

[a] Department of Civil and Environmental Engineering, Michigan Technological University, 1400 Townsend Drive, Dow 854, Houghton, MI 49931, United States
[b] Department of Civil and Environmental Engineering, Michigan Technological University, 1400 Townsend Drive, Dillman 212, Houghton, MI 49931, United States
[c] Department of Civil and Environmental Engineering, Michigan Technological University, 1400 Townsend Drive, Dillman 201F, Houghton, MI 49931, United States

ARTICLE INFO

Keywords:
Spring load restriction
Freeze/thaw depth prediction
Field measurement
Constrained optimization
Freezing/Thawing index

ABSTRACT

Spring Load Restriction (SLR) policies have been widely implemented in many countries to reduce the cost of road repair for freeze-thaw induced damages in cold regions occurring in the spring thawing season. In most SLR policies, accurate predictions of the Freezing Depth (FD) and Thawing Depth (TD) are very critical because both FD and TD directly determine the dates for the SLR initiation and removal. In this study, we propose a new constrained optimization approach to predict FD and TD and evaluate this approach for making SLR decisions with field measurements collected at four sites during two adjacent year cycles. The evaluation results showed that constrained optimization can not only accurately predict FD and TD with a determination coefficient of higher than 0.91 for most sites, but enable FD to meet TD in the thawing season for accurate SLR-decision making, which, however, cannot be achieved using non-constrained optimization widely adopted in the literature. We also discuss the accuracy of using a Thawing Index (TI)/Freezing Index (FI) ratio of 0.3 that still has been used by several agencies in the U.S. to determine the removal date of SLR. Our results indicated that on the true SLR removal dates, a TI/FI ratio is not equal even close to 0.3 for most sites. By comparison, a TI/FI ratio of 0.3 will be less accurate than the FD and TD prediction model for SLR decision-making. The methodology reported in this study is easy to use and implement for road engineers and the insights will help make accurate SLR decisions to prevent roads in cold regions from freeze-thaw induced damages.

Introduction

Paved roads in seasonally cold regions are usually challenged by freeze-thaw induced damages. During a thawing period starting from early spring, the air temperature above a pavement gets warmer and consequently, downward heat transfer to pavement subsurface courses to thaw ice accumulation accumulated during winter in pavement base and subgrade soils [1]. If frozen soils are not completely thawed, the liquid water resulting from thawing could not be quickly drained out of base and subgrade soils, because the water drainage is hindered by the very low permeability of frozen soils [2,3]. In this situation, the soils beneath pavements are under unconsolidated and undrained conditions, which easily leads to mechanical performance degradations in pavement base and subgrade soils [4–6] and consequently causes thaw-weakening [7–9]. This thaw-weakening can significantly cause road damages by reducing their bearing capacity of up to 50% in spring [10–12]. The above issue especially occurs in secondary (low volume) roads, e.g., county roads, city streets, and farm-to-market roads, the majority of which is not designed with enough layer thicknesses to provide adequate protection against freezing and thawing as those in interstate and primary roads [13].

In order to minimize road damages, many regions have implemented Spring Load Restriction (SLR) policies to limit the axle loads of trucks that can significantly induce pavement distortions, cracks, and other damages during annual spring thaw [14,15]. SLR includes initiation and removal dates to create a period for controlling the movement of freight-carrying trucks and heavy equipment travel during this period until the thawing ends to effectively protect roads. Conventional SLR for initiation and removal determinations primarily relies on visual observations in situ, e.g., observing water pumping from cracks or roadway frost deformation [16,17], free water at the pavement surface (indicating a saturated base) to signs of cracking [18], and readings of frost tubes [19].

Despite the above conventional SLR methods, many agencies switch

* Corresponding authors.
E-mail addresses: tbao@mtu.edu (T. Bao), bazmoon@mtu.edu (B. Azmoon), zhenl@mtu.edu (Z. (Leo) Liu).
[1] This work was done at Michigan Technological University, while now working at Pacific Northwest National Laboratory, Richland, WA.

https://doi.org/10.1016/j.trgeo.2020.100419
Received 28 March 2020; Received in revised form 15 July 2020; Accepted 15 August 2020
Available online 25 August 2020

Nomenclature

FD	freezing depth [cm]
FD_{ini}	initial freezing depth [cm]
FI	freezing index [°C-days]
FIT	freezing Index during thawing [°C-days]
TD	thawing depth [cm]
TD_{ini}	initial thawing depth [cm]
TI	thawing index [°C-days]
SLR	spring load restriction [–]

to quantitative SLR decision-making algorithms. Several agencies in the U.S. and Canada have performed research to address the question of monitoring roadways and posting SLR policies using the air Freezing Index (FI) and/or Thawing Index (TI) [19–22]. The SLR initiation, for example, begins when TI reaches 15 °C-days in Manitoba in Canada, while the SLR removal occurs when TI is 350 °C-days [23]. The SLR removal in Washington takes place when the ratio of TI to FI reaches 0.3 [18]. Different from SLR decisions with TI and/or a TI/FI ratio, some agencies currently have recommended determining the initiation and removal of SLR via the Freezing Depth (FD) and Thawing Depth (TD). The reason is that FD and TD can directly reflect real freezing and thawing conditions in pavement base and subgrade soils. For the FD/TD implementation, the SLR initiation starts when TD continuously increases; after TD meets FD in the thawing season, the SLR initiation is removed [24,25]. Therefore, it is very important to accurately predict FD and TD to avoid either the late initiation or early removal of SLR for avoiding any economic loss and reducing the repair cost for road freeze-thaw induced damages.

Many FD and TD prediction models have been proposed in the literature based on 1D heat transfer in a semi-infinite soil. The typical one is the Neumann empirical model [26], where FD is predicted in terms of the square root of FI and soil properties (e.g., thermal conductivity). The following models make some modifications by only keeping FI and lumping all the other terms for soil properties into one or two fitting constants [2,12,16,24]. To obtain these fitting constants, nonlinear regression of the measured data is usually employed. For TD predictions, two major types of prediction models are available in the literature, but each contains 2–4 fitting constants that need to be determined by nonlinear regression as well. The first type is to predict TD via TI only using a power function. Chapin et al. [25], for instance, used this type to predict TD with the measured data, where the obtained determination coefficient was 0.59–0.83. For the second type, TD is assumed to share the same mathematical function as that of FD, i.e., the square root of both FI and TI (see Fig. 1). In comparison, the determination coefficient obtained based upon the second type [24] is about 0.99 and higher than that of the first type. However, Baïz et al. [24] predicted TD in the freezing and thawing seasons separately using a piecewise function, which is inconvenient in practice. Bao et al. [27] thus suggested using an integrated approach to predict TD in the whole freeze-thaw cycle using a multivariate model (i.e., a variation of the second type). They obtained the determination coefficient in a range of 0.8–0.94 and confirmed that the pavement surface temperature is more accurate than the air temperature for calculating FI and TI for FD/TD predictions.

Though either TI or an FD/TD prediction model has been extensively applied for SLR decision-making, two issues are still unclear. Firstly, several agencies in the U.S. still use a ratio of 0.3 between TI and FI proposed by Mahoney et al. [18] to determine the SLR removal date because of its simplicity. However, it is still uncertain how accurately the TI/FI ratio method performs for SLR decision-making when compared to an FD/TD prediction model. Secondly, the essential step in SLR decision-making with an FD/TD prediction model is to determine a date for the SLR removal when FD meets TD (see Fig. 4 for details) in the thawing season [24]. However, FD and TD predicted via the existing model [24] cannot meet with each other, as shown in Fig. 1, which hinders the application of the FD and TD prediction model in practice for SLR decision-making. In addition, when both FI and TI are equal to zero, FD and TD in the thawing season in Fig. 1 are 145 and −848 cm, respectively (22.1 and 0.494 cm in the freezing season). These numbers, in fact, should be identical and have the physical meaning that is related to the pavement surface thickness (see details in Section 'Freeze-thaw depth prediction model with constrained optimization'). Therefore, the fitting constants in Baïz et al. [24] are only statistical numbers without clarifying their physical meaning, which fail to reflect realistic pavement FD and TD conditions.

In this study, we address the above issues using the multivariate FD/TD prediction model adopted from our previous study [27]. Though the prediction model used in this study is the same as that of Bao et al. [27], there are two distinct differences in the model application. First, we clearly clarify the physical meaning of all fitting constants in the prediction model. Second, we propose a new constrained optimization approach for obtaining fitting constants to reflect realistic pavement FD and TD conditions. We evaluate FD and TD predictions with constrained optimization via site measurements collected during two adjacent year cycles in Michigan. Discussion is also made to shed light on the advantages of constrained optimization newly proposed in this study and the SLR decision-making accuracy using the FD/TD prediction model and a TI/FI ratio.

Theory and Method

Field measurements and SLR determination method

Field measurements for road pavements in Michigan are adopted in this study. A Road Weather Information System (RWIS) deployed in Michigan measures and transmits weather and road conditions in real-time via various sensors (Fig. 2). Meteorological sensors record weather conditions, e.g., air temperature, relative humidity, and precipitation. Pavement sensors measure pavement surface temperatures and geo-thermometers are used to measure temperatures of base and subsurface soils. There are 104 sites in total and we adopt four typical sites for analyses, i.e., Michigamme and Seney in the Upper Peninsula and Eastport and Fife Lake in the Lower Peninsula.

Fig. 3 shows the cross-section of the test road pavements. The asphalt/concrete pavement surface has a thickness of about 25 cm, which is the same as that of roads in Asefzadeh et al. [2]. Base and subgrade soils are beneath the surface, where the base thickness is about 17 cm. The degree of frost susceptibility varies with the soil type and usually, silts, clays, and fine silty sands are the most susceptible to frost heave. For all measurement sites in Fig. 2, the soil type is different, which generally includes silty and/or clayey sands, from loose to fine sands, and silty clays. The four selected sites have the soil type as follows:

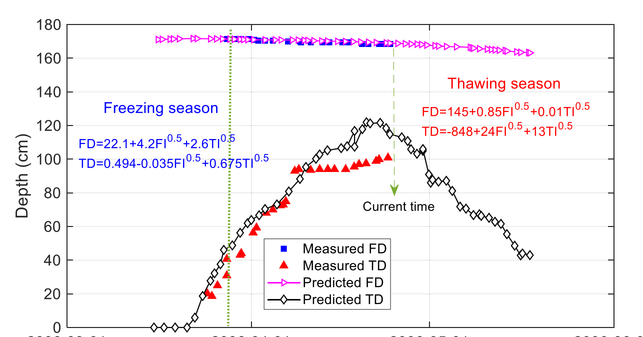

Fig. 1. Measured vs predicted data for FD and TD [data is from Baïz et al. [24]]. Note that predicted TD and FD trends are obtained using the thawing season fitting constants in Baïz et al. [24].

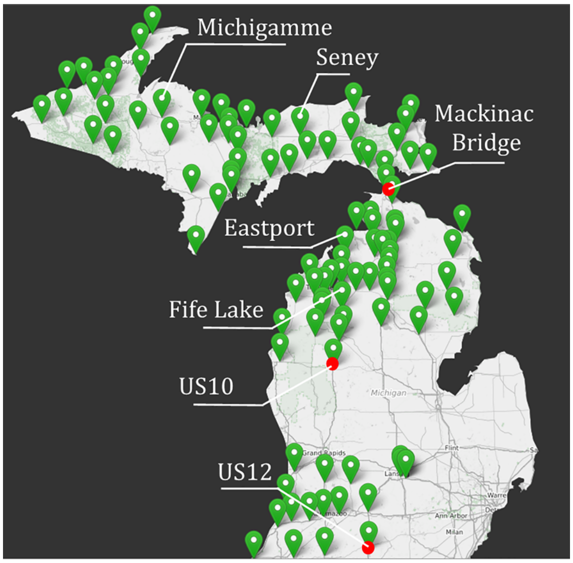

Fig. 2. Monitoring sites in Michigan and selected sites location for analyses. Data is from the Michigan SLR website (https://mdotslr.org/).

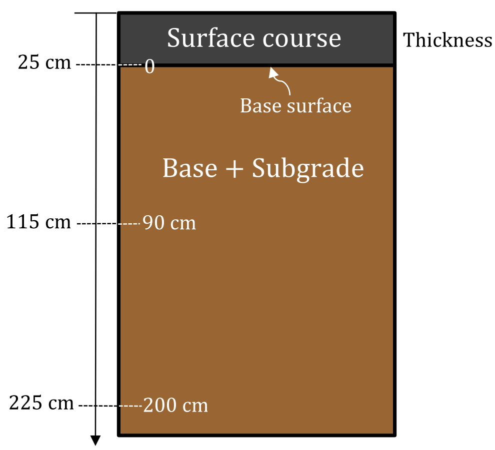

Fig. 3. Schematic of a test road pavement cross section.

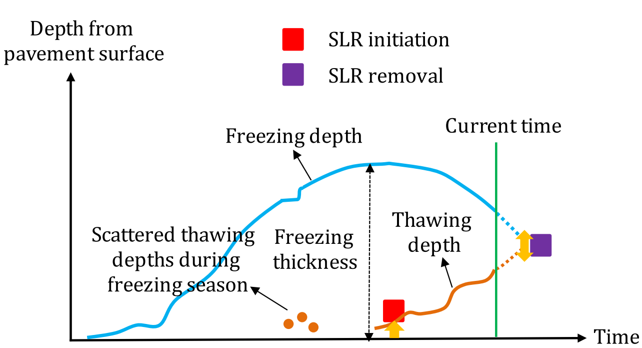

Fig. 4. SLR decision-making based on the theory proposed by [24]. (Note that the model for plotting the FD and TD curves in this figure was derived and simplified based on a mechanistic heat transfer model considering thermal properties of base and subgrade soils. More details can be found in [24;27]. Few scattered TDs can be observed from field measurements (see Fig. 7) before the thawing season, so the SLR initiation begins when continuous TDs can be observed.)

clayey sand upper (~1.52 m) with fine to medium silty sand below at Michigamme, loose sand at Seney, fine sand at Fife Lake, and fine sand upper with silty clay below at Eastport. Thus, the most susceptible soil type is considered. FD and TD are not measured directly, but rather calculated based on the measured subsurface temperatures starting from the base surface to subgrade soils. The measured locations are 0, 3 (7.62), 6 (15.24), 9 (22.86), 12 (30.48), 18 (45.72), 24 (60.96), 30 (76.2), 36 (91.44), 42 (106.68), 48 (121.92), 54 (137.16), 60 (152.4), 66 (167.64), and 72 in. (182.88 cm). Calculations of FD and TD are defined based on measured temperatures with respect to 0 °C from the top surface (i.e., base surface in Fig. 3) during freezing and thawing periods. Two adjacent measured temperatures are compared with 0 °C and the linear interpolation is used if two adjacent temperatures have an opposite sign. The base surface in Fig. 3 is assumed as a datum, below which FD and TD are positive.

The SLR initiation and removal dates are determined according to the suggested theory by Baïz et al. [24] and Chapin et al. [25]. As shown in Fig. 4, the SLR initiation takes place if there are continuous TDs (red square); SLR ends after TD meets FD (purple square). At this time, a yearly freeze-thaw cycle is complete.

Freeze-thaw depth prediction model with constrained optimization

Accurate predictions of FD and TD are very essential for SLR decision-making to notify the public of SLR postings at least 3–5 days in advance for avoiding the economic loss of road users due to an unnecessarily long SLR period. In this study, we adopt the multivariate FD/TD prediction model [27]. This model assumes that FD is a function of the square root of both FI and TI as

$$FD = a\sqrt{FI} + \sqrt{c - bTI} - d \tag{1}$$

where a, b, c, and d are fitting constants, all are always positive. The mathematical formulation for TD uses the square root function using the following expression by assuming that freezing and thawing processes in soils are similar [28]

$$TD = -e\sqrt{FIT} - \sqrt{g - fTI} + h \tag{2}$$

where e, g, f, and h are fitting constants, all are always positive. FIT is the cumulative freezing index in the thawing period only, which is calculated starting from the first TD data point. Detailed calculations of FI, FIT, and TI can be found in Appendix.

Each of Eqs. (1) and (2) has four fitting constants. For FD, a and b are the lumped parameters in the freezing and thawing seasons, respectively, to consider the volumetric latent heat of fusion, the conversion from the air temperature to the surface temperature, and the initial freezing depression [29,30]. These two lumped fitting constants reflect the real situation for the depth and duration of the freeze and thaw penetration in the base and subgrade soils. Similarly, e and f for TD are also the lumped parameters that have a similar physical meaning to that of a and b.

The physical meaning of c and d in Eq. (1) is related to the pavement surface thickness. Before the freezing season starts, it is known that both FI and TI are equal to zero. Eq. (1) thus can be rewritten as

$$FD_{ini} = \sqrt{c} - d \tag{3}$$

where FD_{ini} the initial freezing depth to represent the pavement surface thickness. In Fig. 3, the base surface is the datum. FD starts from zero in the early freezing stage when FI is slightly greater than zero and TI is equal to zero. FD only occurs in base and subgrade soils beneath the pavement surface (Fig. 3). Under the condition of FI = TI = 0, FD_{ini} needs to be equal to 25 cm such that realistic pavement structure conditions can be physically described using Eq. (1). Similarly, Eq. (2) for TD can be written as

$$TD_{ini} = -\sqrt{g} + h \tag{4}$$

Because of the same pavement road, $FD_{ini} = TD_{ini}$ is required. The above explanations give the physical meaning of all the fitting constants in Eqs. (1)–(2) in the multivariate FD/TD model. This is different from the existing prediction models that conduct regression analyses directly to have fitting constants; however, their fitting constants fail to reflect

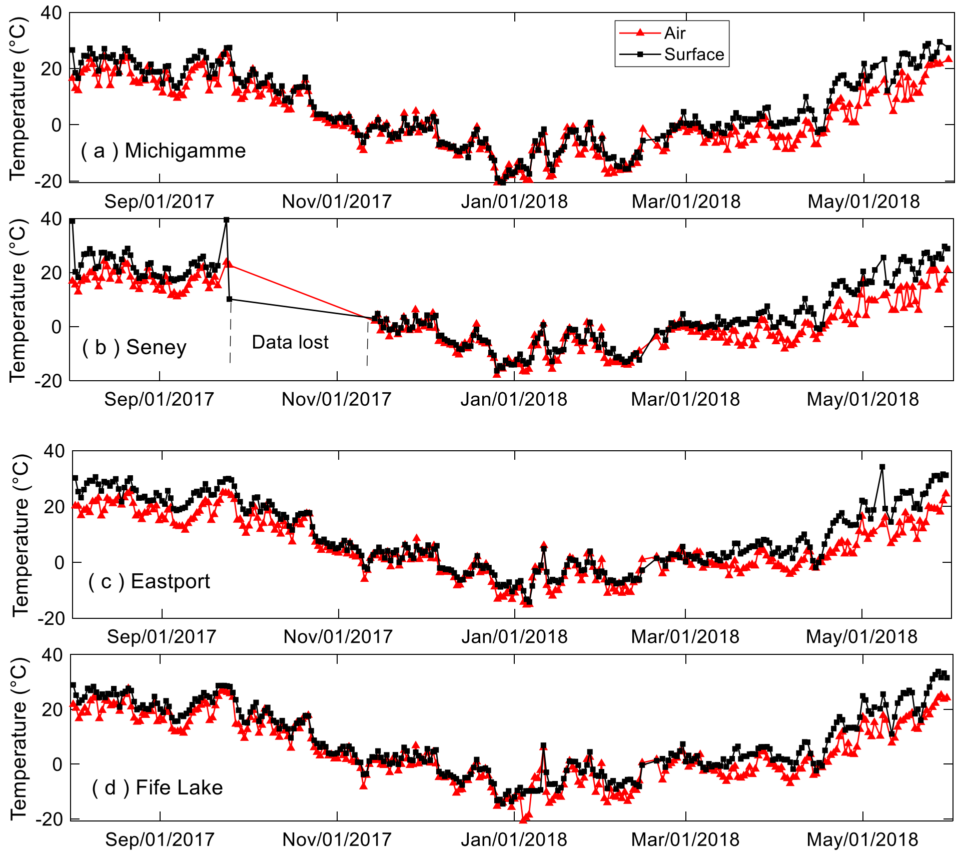

Fig. 5. Measured air and pavement surface temperatures for Year Cycle 2017–2018.

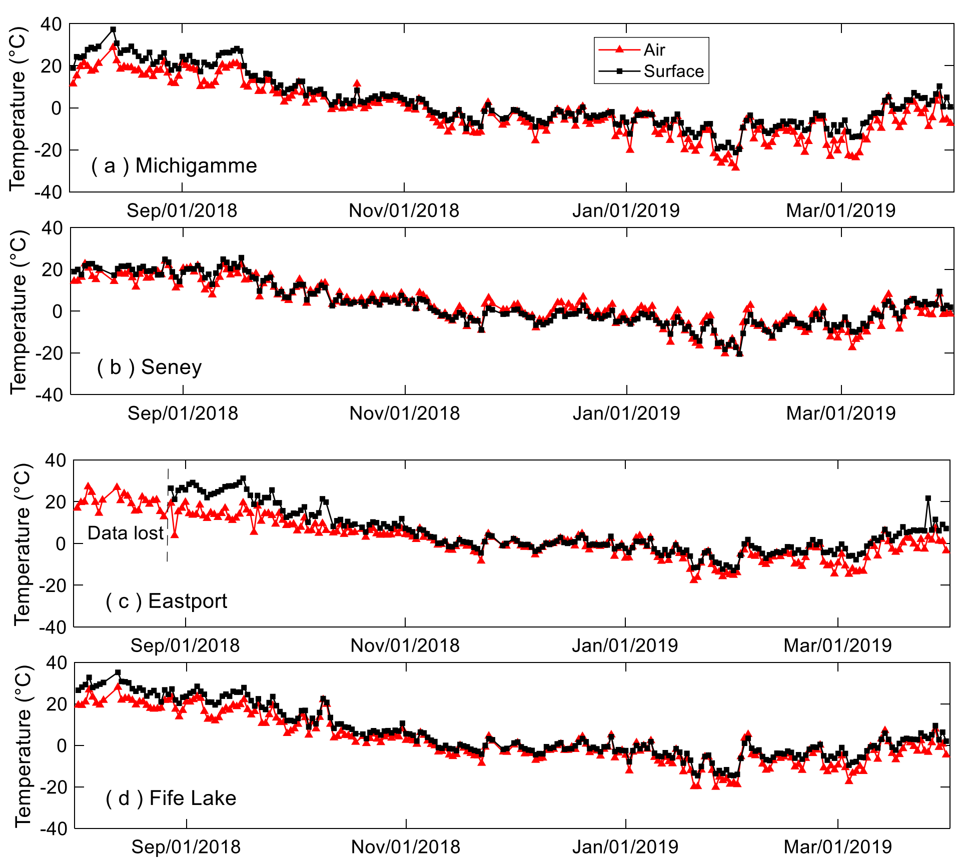

Fig. 6. Measured air and pavement surface temperatures for Year Cycle 2018–2019.

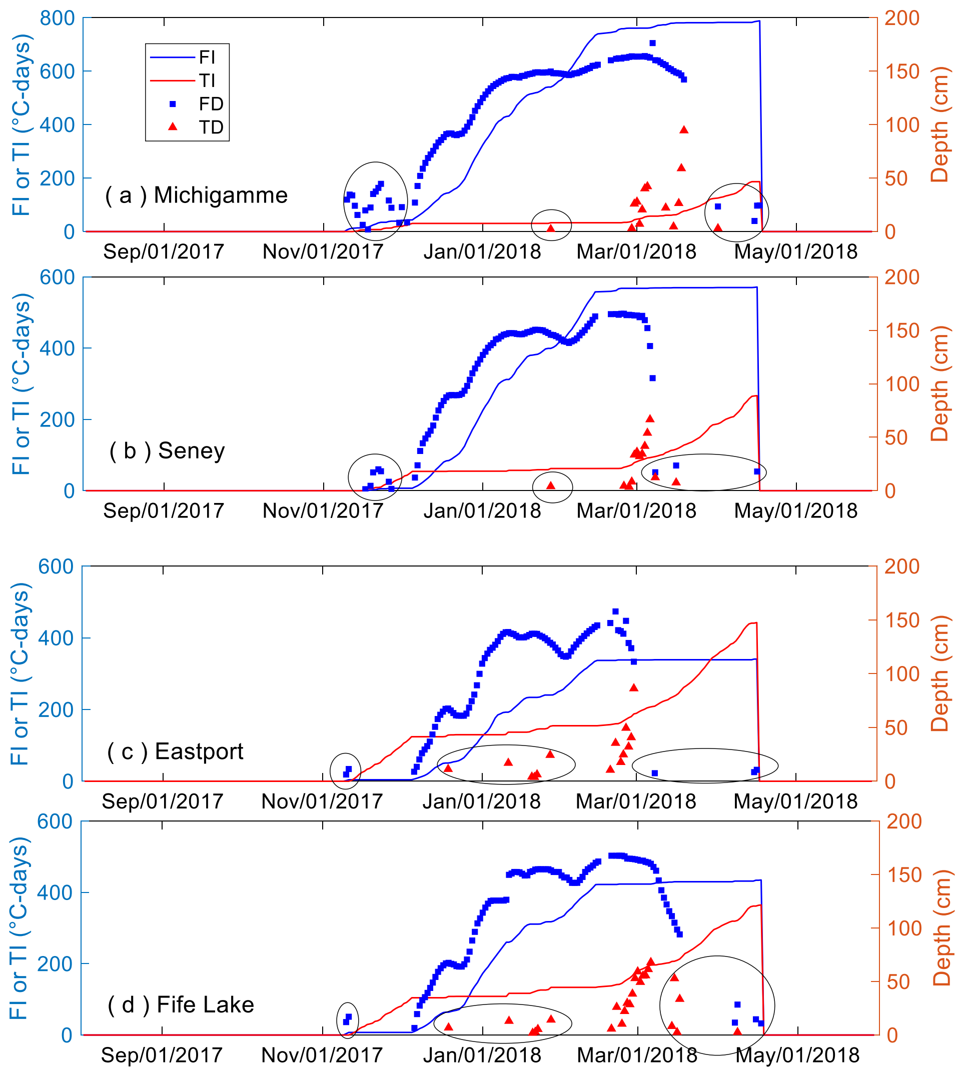

Fig. 7. Measured FDs and TDs with FI/TI calculated using the pavement surface temperature for Year Cycle 2017–2018. Data within circles will be excluded in the fitting analysis.

realistic pavement conditions (e.g., Baïz et al. [24] and Chapin et al. [25], see an example in Fig. 1).

Non-constrained nonlinear regression of measured data is widely used to find fitting constants in the FD/TD prediction models [2,12,16,24]. However, non-constrained nonlinear regression cannot satisfy the requirements of Eqs. (3)–(4) in this study. We thus propose a new constrained optimization approach to satisfy such requirements. In theory, the minimum of a nonlinear multivariable function $f(\boldsymbol{x})$ can be expressed as [31]

$$\min_{\boldsymbol{x}} f(\boldsymbol{x}) \text{ such that} \begin{cases} \boldsymbol{x} \geqslant 0 \\ ceq(\boldsymbol{x}) = 0 \end{cases} \tag{5}$$

where $\boldsymbol{x}$ is the fitting constant vector and $ceq(\boldsymbol{x})$ is the equality constraints. Take FD for example, $\boldsymbol{x}$ contains a, b, c, and d. $f(\boldsymbol{x})$ and $ceq(\boldsymbol{x})$ can be expressed as

$$\begin{cases} f(\boldsymbol{x}) = \sum [FD(\boldsymbol{x}) - g(\boldsymbol{x})]^2 \\ ceq(\boldsymbol{x}) = \sqrt{c} - d - FD_{ini} \end{cases} \tag{6}$$

where $g(\boldsymbol{x})$ is the measured data vector. In this study, $FD_{ini} = TD_{ini} = -25$ cm is used (Fig. 3). We utilize the negative sign here because the base surface is the datum. The constrained optimization procedure is shown in Flowchart 1. This constrained nonlinear optimization is implemented with MATLAB using the *fmincon* method for optimization construction and sequential quadratic programming (SQP) algorithm [32] for finding the minimum of $f(\boldsymbol{x})$. The randomly generated $\boldsymbol{x}$ is used to start the optimization process and the termination tolerance for $f(\boldsymbol{x})$ is 10^{-12}.

Flowchart 1. Constrained optimization procedure

Given: TD or FD measurements
Output: Model parameters a, b, c, and d for FD or e, f, g, and h for TD

Step 1. Give initial guesses for model parameters in [0 Infinite].
Step 2. Do optimization with constraints (e.g., $ceq(\boldsymbol{x}) = \sqrt{c} - d - FD_{ini}$).
Step 3. Evaluate $f(\boldsymbol{x})$; if its tolerance is not satisfied, adjust initial guesses using the SQP algorithm and repeat Step 2, otherwise do Step 4.
Step 4. Report model parameters for FD or TD.

Results

Site measurements

Two year-cycle field data for the four considered sites are available to evaluate the FD/TD model performance with constrained optimization. Fig. 5 and Fig. 6 show the daily average air and pavement surface temperatures collected from August 1st 2017 to June 1st 2018 for the first year cycle and August 1st 2018 to April 1st 2019 for the second

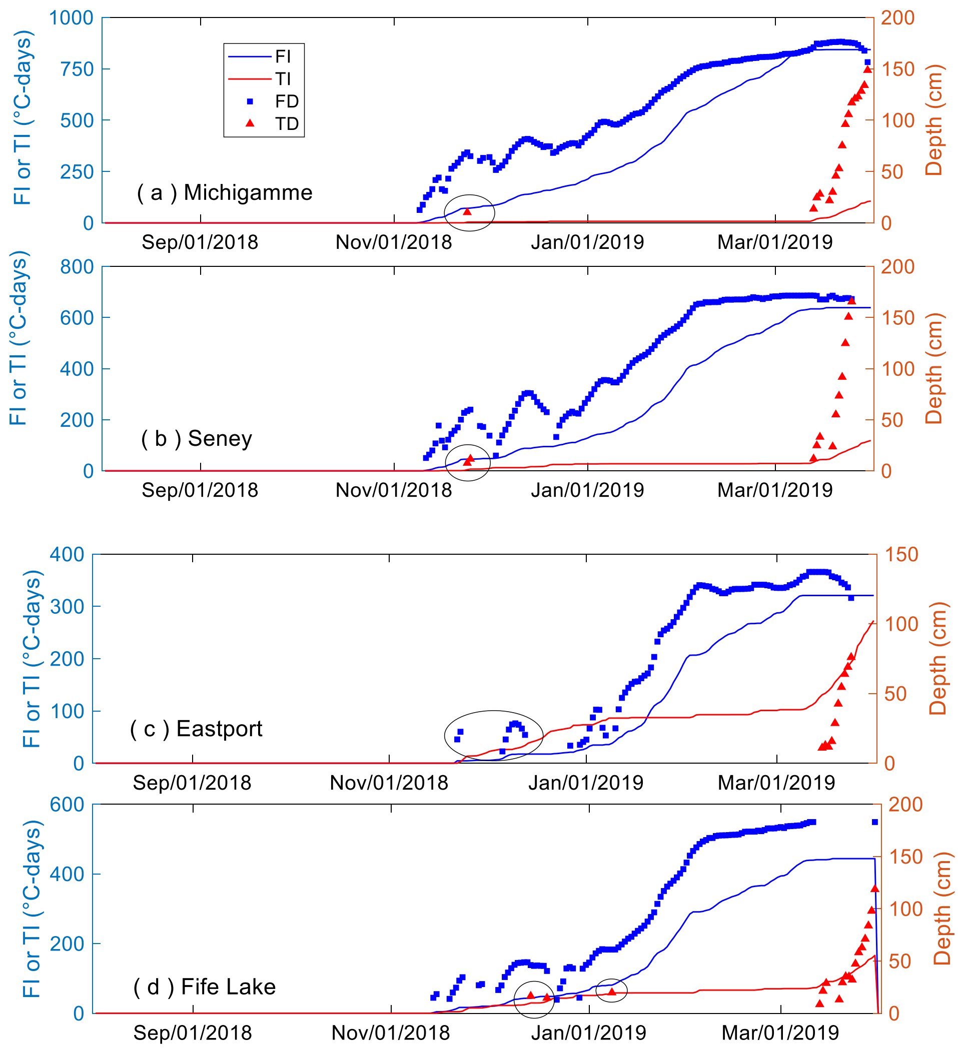

Fig. 8. Measured FDs and TDs with FI/TI calculated using the pavement surface temperature for Year Cycle 2018–2019. Data within circles will be excluded in the fitting analysis.

year cycle. The second year cycle has less data than the first year cycle primarily due to problems caused by the data transmission. The data after April 1st 2019 is not available. In general, the surface temperature is slightly higher than the air temperature. Also, the temperature range for the two-year cycles is almost the same from −20 °C to 40 °C. In Fig. 5b and Fig. 6c, some data is missing in a short period probably because of the sensor connection and data transmission problems. This, however, does not affect TD predictions and may only slightly affect FD predictions in the early stage. We can see the continuous data after about November 15th, 2017. Thus, TD predictions are negligibly affected by the missing data for SLR decision-making.

The measured FDs and TDs for the four sites for the two-year cycles are shown in Figs. 7–8. FI and TI are also plotted, which are calculated starting from the first FD data point with the pavement surface temperature using Eqs. (7)–(8) detailed in Appendix. In all the sites, FD takes place around November 15th for each year cycle. The thawing season for the first year cycle is earlier than that of the second year cycle. Because we can see that FD starts decreasing around the beginning of March in Fig. 7 but around the middle of March in Fig. 8. This can also be supported by TD prediction trends. TD continuously increases around the beginning of March for the first year cycle but around the middle of March for the second year cycle. For all the sites in Fig. 7 and Fig. 8, there are some data points marked with circles. This can be explained in terms of two seasons. In the freezing season, several warm days may occur to thaw the base and subgrade soils; as a result, FD decreases somewhat, especially at the beginning of the freezing season. In the thawing season after the freeze-thaw cycle ends where FD meets TD, there have some cold days to freeze the soils close to the base surface, leading to some FDs after the freeze-thaw cycle ends.

Application of constrained optimization for FD/TD predictions

Predictions of FD and TD via constrained optimization for the two-year cycles are shown in Fig. 9 and Fig. 10. During the constrained optimization process, the circled data marked in Figs. 7–8 is excluded. The major consideration is that the circled data appears either at the beginning of the freezing season or after the thawing season due to the occurrence of some warm and/or cold days, as explained in Section ‘Site measurements’. The primary aim of this study is to predict TD and FD trends in the thawing season for accurately making SLR decisions. It is thus reasonable to exclude the circled data for statistical analyses to obtain high prediction accuracy in the thawing season.

We can see in Figs. 9-10 that the predicted data for both FD and TD is in good agreement with the measured data. In general, the predicted FD trends match well with the measured FD trends, where FD increases in the freezing season and decreases when thawing starts. Slight deviations for FD can be observed in Fig. 10 in a few days at the beginning of the freezing season because of the occurrence of some warm and/or cold days. This, however, has a negligible effect because the predicted FDs in the thawing season, which are key for determining the SLR

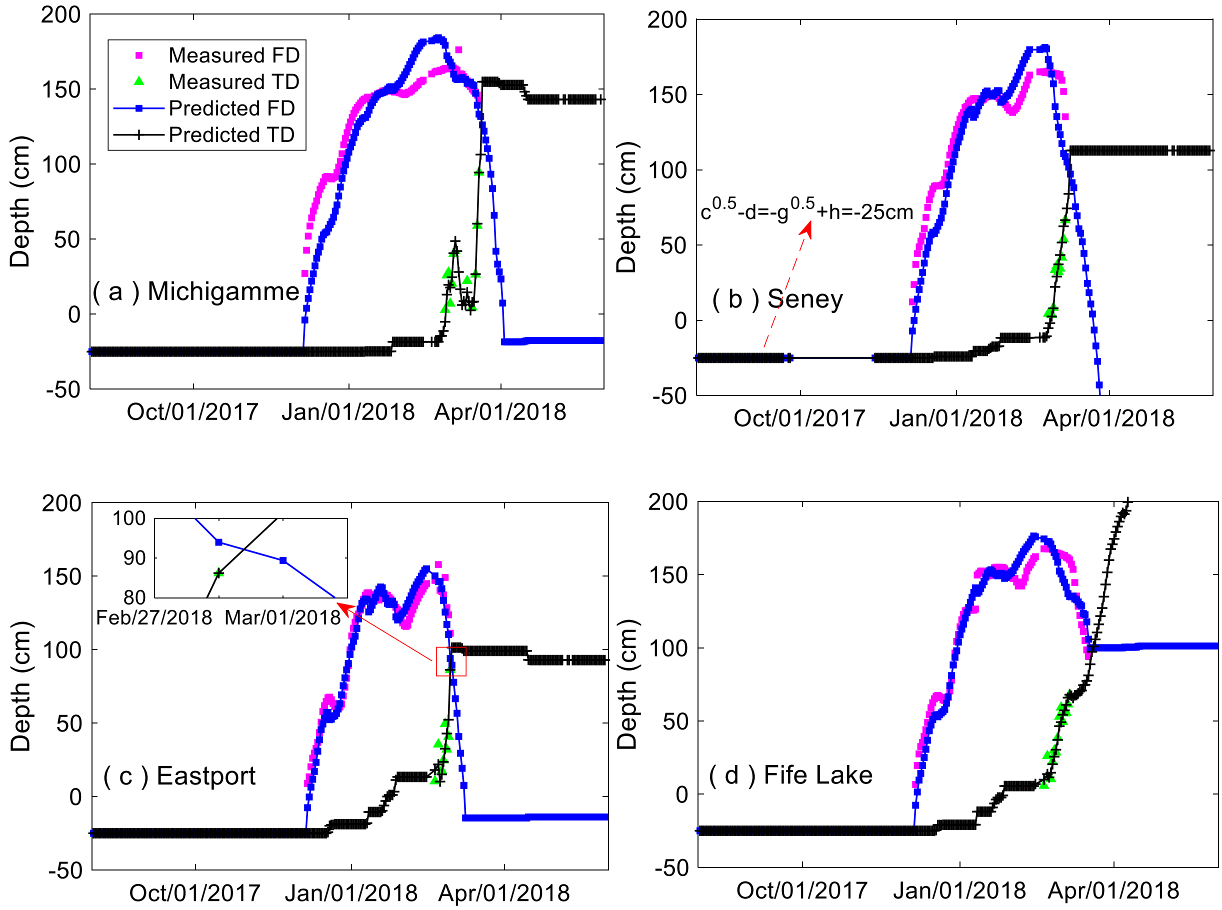

Fig. 9. Predictions of FD and TD with the measured data for Year Cycle 2017–2018. Circled data in Fig. 7 is excluded.

removal date, are very close to the measured FDs. It is also seen that FD and/or TD is a horizontal line after FD meets TD because imaginary numbers are obtained using Eqs. (1)–(2). This, however, is not an issue because the freeze-thaw cycle ends already, thus, these FD and/or TD values have no meaning.

The fitting constants for TD and FD are tabulated in Table 1. All the fitting constants are positive, which satisfy the requirement of constrained optimization in Eq. (5). The determination coefficient for almost all the predictions is found to be higher than 0.91, which further confirms the high accuracy of predicting both FD and TD with constrained optimization. In Figs. 9–10, we also can see FD and TD are overlapped and equal to −25 cm in the early freezing season when no measured FD data point appears. This satisfies Eq. (6) for the physical meaning of the fitting constants to reflect the pavement surface thickness. At the late stage of the thawing season, FD meets TD in the predictions for all the sites, except Fife Lake in the second year cycle because no more data is available after April 1st. However, it is expected that FD will meet TD later according to their current prediction trends in Fig. 10d.

The initiation and removal of SLR for the four sites then can be determined according to Fig. 4. As shown in Table 2, all the sites in the first year cycle have an earlier date for the SLR initiation and a later date for the SLR removal than the second year cycle. This is because the thawing season of the first year cycle came earlier (see Figs. 7–8). The FD/TD model suggests that the duration for SLR in Michiganmme is 22 days for the first year cycle and 20 days for the second year cycle. For the other three sites, the SLR duration is 17, 10, and 29 for the first year cycle and 13, 11, and not determined for the second year cycle, respectively. Considering that there are a few warms and/or cold days after FD meets TD when the freeze–thaw cycle ends (Fig. 7), it is also suggested that the removal of SLR can take place when no more TD data point appears to eliminate any potential of thaw-weakening induced road damages. Such suggested dates for the SLR removal are shown in Table 2 and we can see that the SLR duration of the first year cycle increases over one or two weeks in Michigamme, Seney, and Fife Lake, while the SLR duration in Eastport keeps unchanged.

Discussion

Advantages of using constrained optimization for FD/TD predictions

Constrained optimization has two major advantages that make it more advanced than non-constrained optimization used in existing studies [24,27] for statistical analyses of the measured data. First, as clearly shown in Figs. 9–10, constrained optimization can enable FD to meet TD in the thawing season. This can be further illustrated by comparing FD and TD predictions with non-constrained and constrained optimizations. Fig. 11 shows such a comparison for the statistical analyses of the data collected during 2017–2018 in Seney. We can see that FD cannot meet TD in the thawing season if non-constrained optimization is employed, which has the same issue pointed out in Fig. 1. However, constrained optimization can resolve this issue to enable the prediction model to work in practice in support of SLR decision-making.

Second, when FI = TI = 0 in the early freezing season, non-constrained optimization yields about −5 cm and 25 cm (Fig. 11) for TD and FD, respectively. The two numbers are different and also have a different sign simply resulting from the statistical analyses. They, however, cannot reflect the realistic pavement FD and TD conditions. As explained in Section ‘Freeze-thaw depth prediction model with

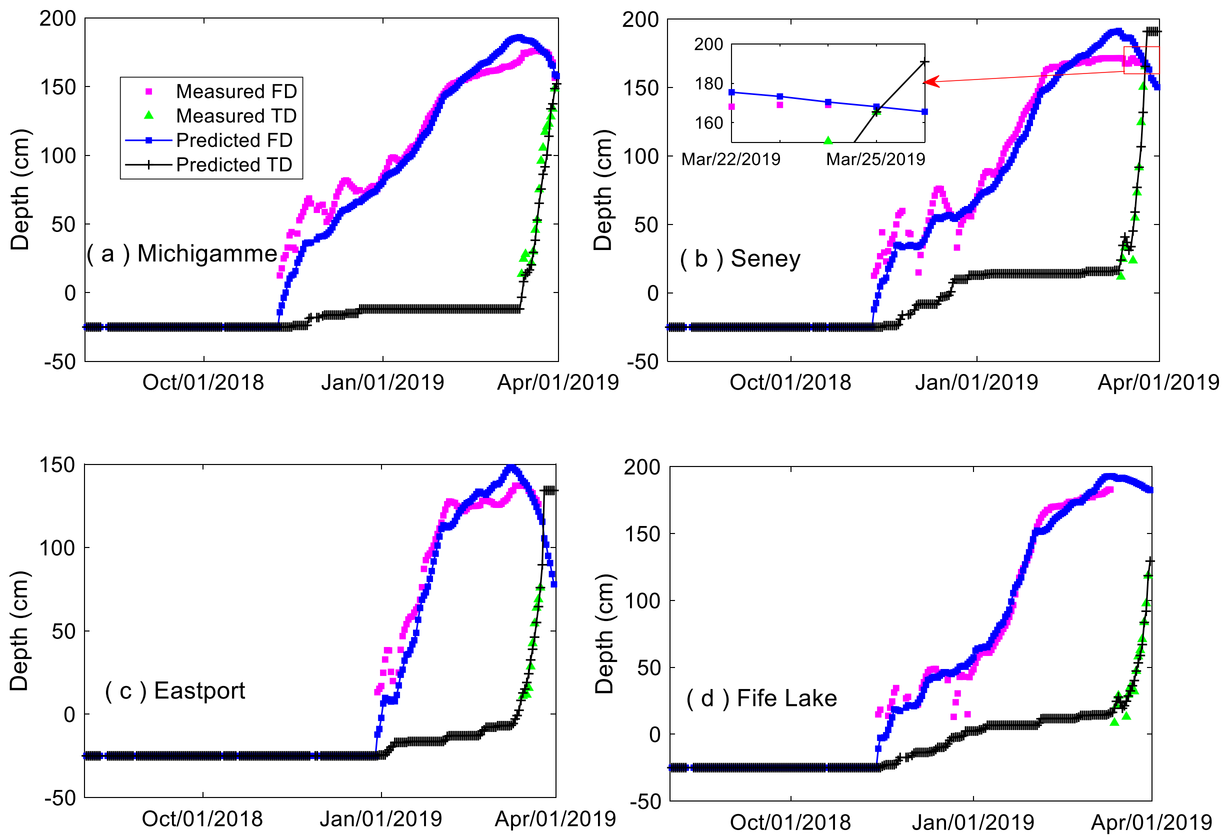

Fig. 10. Predictions of FD and TD with the measured data for Year Cycle 2018–2019. Circled data in Fig. 8 is excluded.

Table 1
Fitting results for FD and TD.

Site	Year cycle	Fitting constant for FD				
		a (cm °C-day$^{-0.5}$)	b (cm^2 °C-day^{-1})	c (cm^2)	d (cm)	R^2
Michigamme	2017-2018	7.93	441.68	43671.34	233.98	0.9454
	2018-2019	7.36	37.70	5942.01	102.11	0.9826
Seney	2017-2018	9.55	1129212.34	55527423258.98	235667.58	0.9175
	2018-2019	8.99	66.89	10452.05	127.24	0.9667
Eastport	2017-2018	12.24	765988.37	77196409094.82	277867.42	0.9695
	2018-2019	10.53	64.56	14750.30	146.45	0.9738
Fife Lake	2017-2018	10.54	77.03	8406.61	116.69	0.9460
	2018-2019	10.79	35597.02	23217827654.84	152398.97	0.9764
		Fitting constant for TD				
		e (cm °C-day$^{-0.5}$)	f (cm^2 °C-day^{-1})	g (cm^2)	h (cm)	R^2
Michigamme	2017-2018	16.08	1289.25	63770.78	227.53	0.9337
	2018-2019	0.0005	2234315.90	448425887174.61	669621.09	0.9601
Seney	2017-2018	0	437.21	18992.62	112.81	0.9160
	2018-2019	5.01	583.89	51533.68	202.01	0.9745
Eastport	2017-2018	10.70	299.15	19229.11	113.67	0.8085
	2018-2019	0.66	182.23	25366.36	134.27	0.9651
Fife Lake	2017-2018	2.71	1714226.75	671747443635.23	819577.00	0.9212
	2018-2019	5.07	160.17	26692.41	138.38	0.9777

constrained optimization', these two numbers should be equal because they represent the pavement surface thickness. It is clearly seen in Fig. 11 that FD is equal to TD when constrained optimization is used. Therefore, constrained optimization can yield not only satisfactory but more realistic results than those obtained with non-constrained optimization.

Feasibility of using Year Cycle 1 fitting constants to predict Year Cycle 2 FD/TD

The FD/TD prediction model with constrained optimization can accurately predict the FD/TD trends for applying SLR in each year cycle. It is also very interesting to explore the feasibility of predicting the FD and TD trends in the current year cycle by directly employing the fitting constants from the previous year cycle at the same site. This feasibility can further facilitate the application of the prediction model

Table 2
Site SLR determination.

Site	Year cycle	Model determined date			Suggested date	
		SLR on	SLR off	Duration (days)	SLR off	Duration (days)
Michigamme	2017–2018	2/27/2018	3/20/2018	22	4/2/2018	35
	2018–2019	3/13/2019	4/1/2019	20	4/1/2019	20
Seney	2017–2018	2/24/2018	3/9/2018	17	3/16/2018	24
	2018–2019	3/13/2019	3/25/2019	13	3/25/2019	13
Eastport	2017–2018	2/19/2018	3/1/2018	10	3/1/2018	10
	2018–2019	3/15/2019	3/25/2019	11	3/25/2019	11
Fife Lake	2017–2018	2/19/2018	3/20/2018	29	4/8/2019	48
	2018–2019	3/13/2019	–	–	–	–

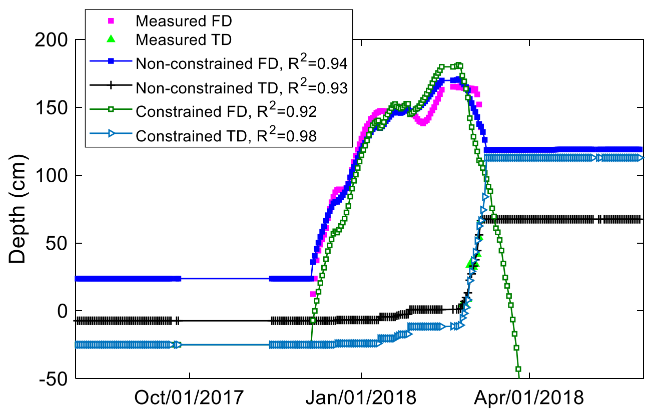

Fig. 11. Comparison of FD/TD predictions with non-constrained and constrained optimization for Seney during 2017–2018.

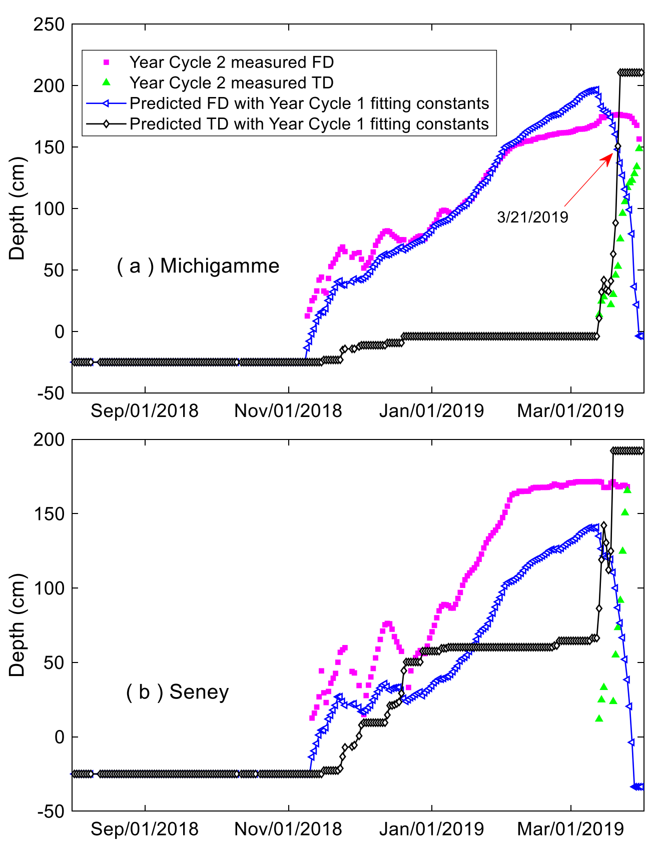

Fig. 12. Comparison of FD/TD predictions with non-constrained and constrained optimization in Seney for Year Cycle 2017–2018.

in practice because it makes the model application more convenient for road engineers for making SLR decisions without needing further measurements in later year cycles.

To examine this feasibility, we predict the FD and TD trends during 2018–2019 in Michigamme and Seney, respectively, using the fitting constants obtained during 2017–2018 from Table 1. As shown in Fig. 12, the predictions for both FD and TD lag behind and do not match the measured data. The SLR removal for Michigamme is determined on 3/21/2019, which is earlier than the correct date of 4/1/2019. The SLR removal for Seney is also earlier and incorrect. The major reason for causing the earlier predictions is that the thawing season during 2017–2018 is earlier than that during 2018–2019 (see Figs. 7-8). Therefore, it is not suggested to predict the FD and TD trends in the current year cycle using the fitting constants from the previous year cycle. Though at the same site, the accuracy of the TD and FD predictions is also time-dependent and significantly influenced by FI and TI accumulated during each year cycle.

FD/TD prediction models are better than a TI/FI ratio for SLR decision-making

As mentioned in the introduction, a TI/FI ratio of 0.3 proposed by Mahoney et al. [18] has still been used by several agencies in the U.S. to determine the SLR removal date, e.g., those in Washington [18,33]. In this section, we evaluate the accuracy of using this TI/FI ratio for SLR decision-making.

Table 3 shows TI/FI ratios calculated by TI and FI obtained on the SLR removal dates. The removal dates are determined based upon the measured data in Figs. 9–10 when FD either already or nearly meets TD. These dates can be considered as the true solutions for removing SLR because the field measurements directly reflect pavement freezing and thawing conditions. TI/FI ratios for Eastport and Fife Lake are not either fully or partially shown in Table 3. The reason is that the last FD and TD data points at these two sites in Figs. 9–10 are still far from each other; therefore, it is difficult to determine the correct SLR removal dates. The SLR removal dates determined by the FD/TD prediction model are also presented for comparison. We can see in Table 3 that the TI/FI ratios are not equal and/or very close to 0.3. Even at the same site, the ratio is obviously different in the two-year cycles. This might be caused by two possible reasons. First, FI and TI in Table 3 are calculated in terms of the pavement surface temperature. This differs from the air temperature used in Mahoney et al. [18] for obtaining a TI/FI ratio of 0.3. Second, Mahoney et al. [18] used “°F” for the temperature unit while “°C” is utilized here.

To further examine the accuracy of using the TI/FI ratio, we calculate the TI/FI ratios for three additional sites in the Superior region in Michigan (see Fig. 2), including Mackinac Bridge, US-10, and US-12. In the calculation, we adopt the air temperature to compute FI and TI using both “°F” and “°C” temperature units. The SLR removal dates are determined based upon the field measurements when FD meets TD. It is

Table 3
Ratios between TI and FI on the SLR removal date.

Site	Year circle	FI (°C-day)	TI (°C-day)	TI/FI ratio	SLR off	
					Measurement	FD/TD model
Michigamme	2017–2018	737.68	47.64	0.06	3/19/2018	3/20/2018
	2018–2019	843.32	106.13	0.13	4/1/2019	4/1/2019
Seney	2017–2018	561.87	43.46	0.08	3/6/2018	3/9/2018
	2018–2019	638.67	87.14	0.14	3/25/2019	3/25/2019
Eastport	2017–2018	334.25	65.38	0.20	2/28/2018	3/1/2018
	2018–2019	–	–	–	–	3/25/2019
Fife Lake	2017–2018	–	–	–	–	3/20/2018
	2018–2019	–	–	–	–	–

Table 4
SLR removal dates at three additional sites in the Superior region in Michigan.

Site	Year	Date SLR off	FI		TI		TI/FI ratio	
			°F-day	°C-day	°F-day	°C-day	if °F	if °C
Mackinac Bridge	2017	4/5/2017	694.00	477.22	362.00	201.33	0.52	0.42
	2014	5/4/2014	2024.00	1267.80	528.00	293.56	0.26	0.23
	2011	4/18/2011	1062.00	711.67	1180.00	655.92	1.11	0.92
US-10	2017	3/23/2017	471.00	330.56	498.00	276.90	1.06	0.84
US-12	2017	3/8/2017	298.00	211.11	706.00	392.48	2.37	1.86

clearly seen in Table 4 that the TI/FI ratio is not equal or close to 0.3 for most sites, no matter "°F" or "°C" is utilized. The TI/FI ratio is in a range of 0.26–2.37 when "°F" is used.

The results in Table 3 and Table 4 show that adopting a TI/FI ratio of 0.3 is not accurate for SLR decision-making. Even at the same site of Mackinac Bridge, the TI/FI ratio is significantly different in three considered years (Table 4). However, the SLR removal dates determined by the FD/TD prediction model are almost the same as those by the measurements (Table 3). According to Mahoney et al. [18], a TI/FI ratio of 0.3, in fact, is an approximate solution under cases based upon fine-grained soils with a moisture content of 0.15. This approximate solution, however, can vary significantly site-by-site or year-by-year though at the same site. Using this approximate TI/FI ratio will yield an SLR removal date either earlier or later than a true date. This will cause the extra repair cost for freeze-thaw-induced road damages occurring in the thawing season or the economic loss of road users due to an unnecessarily long SLR period. Our results reveal that the FD and TD prediction model can yield more accurate results than a TI/FI ratio for SLR decision-making.

Conclusions

This study proposes constrained optimization to predict FD and TD in support of making SLR decisions. The physical meanings of all fitting constants in the multivariate FD/TD prediction model are clearly clarified, which can reflect realistic pavement FD and TD conditions but are conventionally neglected in existing studies. We evaluate constrained optimization with field measurements collected at four sites during two-year cycles. The evaluation results showed that the constrained optimization approach can provide accurate predictions of FD and TD with the determination coefficient of higher than 0.91 for almost all sites. Most importantly, this approach makes the predicted FD and TD trends cross in the thawing season so that the SLR removal date can be determined, which addresses the critical but resolved issue in most existing prediction models that FD cannot meet TD in the thawing season to enable such prediction models to work in practice for SLR decision-making.

Based on the examination, it is not suggested to predict the FD and TD trends in the current year cycle by directly employing the fitting constants from the previous year cycle at the same site. By comparison, the FD and TD prediction model used in this study is more accurate for SLR decision-making than a TI/FI ratio of 0.3 that still has been used in several agencies in the U.S. The TI/FI ratio can vary significantly site-by-site or year-by-year though at the same site. Therefore, the FD and TD prediction model with constrained optimization reported in this study is reliable and highly recommended for making SLR decisions for roadways in cold regions.

CRediT authorship contribution statement

Ting Bao: Conceptualization, Methodology, Data curation, Writing - original draft. **Behnam Azmoon:** Formal analysis, Resources. **Zhen (Leo) Liu:** Writing - review & editing.

Declaration of Competing Interest

The authors declare that they have no known competing financial interests or personal relationships that could have appeared to influence the work reported in this paper.

Acknowledgments

This research is supported by the Michigan Department of Transportation (MDOT OR 16-009).

Appendix A

Freezing and thawing indices calculation

The cumulative freezing index is calculated based on $T_0 = 0$ °C during a given period by the following expression

$$\begin{cases} FI = \sum (T_0 - T_s) \\ T_0 - T_s < 0 \Rightarrow T_0 - T_s = 0 \end{cases} \tag{7}$$

where T_s is the pavement surface temperature (note that T_s is the daily averaged data from Figs. 5 and 6). Similarly, FIT is calculated using Eq. (7) starting from the date when the first TD data point occurs in the thawing season only. The cumulative thawing index is computed by

$$\begin{cases} TI = \sum (T_s - T_{ref}) \\ T_s - T_{ref} < 0 \Rightarrow T_s - T_{ref} = 0 \end{cases} \tag{8}$$

where T_{ref} is the reference temperature to consider the amount of solar radiation and thermal properties of pavement materials. $T_{ref} = -1.67$ °C is often utilized according to the guideline in Mahoney et al. [18].

References

[1] Xu F, Song W, Zhang Y, Li B, Hu Y, Kim Y, et al. Water content variations during unsaturated feet-scale soil freezing and thawing. Cold Reg Sci Technol 2019;162:96–103.
[2] Asefzadeh A, Hashemian L, Haghi NT, Bayat A. Evaluation of spring load restrictions and winter weight premium duration prediction methods in cold regions according to field data. Can J Civ Eng 2016;43:667–74.
[3] Chamberlain EJ, Gow AJ. Effect of freezing and thawing on the permeability and structure of soils. Eng Geol 1979;13:73–92.
[4] Ishikawa T, Lin T, Kawabata S, Kameyama S, Tokoro T. Effect evaluation of freeze-thaw on resilient modulus of unsaturated granular base course material in pavement. Transp Geotech 2019;21:100284.
[5] Nguyen TTH, Cui Y-J, Ferber V, Herrier G, Ozturk T, Plier F, et al. Effect of freeze-thaw cycles on mechanical strength of lime-treated fine-grained soils. Transp Geotech 2019;21:100281.
[6] Domitrović J, Rukavina T, Lenart S. Effect of freeze-thaw cycles on the resilient moduli and permanent deformation of RAP/natural aggregate unbound base mixtures. Transp Geotech 2019;18:83–91.
[7] Simonsen E, Isacsson U. Thaw weakening of pavement structures in cold regions. Cold Reg Sci Technol 1999;29:135–51.
[8] Shoop S, Affleck R, Haehnel R, Janoo V. Mechanical behavior modeling of thaw-weakened soil. Cold Reg Sci Technol 2008;52:191–206.
[9] Lu Z, She J, Wu X, Yao H. Cumulative strain characteristics of compacted soil under effect of freeze-thaw cycles with water supply. Transp Geotech 2019;21:100291.
[10] Isotalo J. Seasonal truck-load restrictions and road maintenance in countries with cold climate. Transport, Water Urban Dev Department 1993:1–7.
[11] Ningyuan L, Eng P, Kazmierowski T, Lane B. Long-term monitoring of low-volume road performance in Ontario. In: Annual Conference and Exhibition of the Transportation Association of Canada: Transportation without Boundaries. Ottawa, Canada; 2006.
[12] Miller H, Cabral C, Kestler M, Berg R, Eaton R. Calibration of a freeze-thaw prediction model for spring load restriction timing in northern New England. Cold Regions Engineering 2012: Sustainable Infrastructure Development in a Changing Cold Environment. Quebec City, Canada: American Society of Civil Engineers; 2012. p. 369–79.
[13] Baladi GY, Rajaei P. Predictive modeling of freezing and thawing of frost-susceptible soils. Lansing, MI: Michigan State University, Department of Civil & Environmental Engineering; 2015.
[14] Huen K, Tighe S, Mills B, Perchanok M. Development of tools for improved spring load restriction policies in Ontario. The Annual conference of the Transportation Association of Canada (TAC). Charlottetown, Prince Edward Island; 2006. p. 1–16.
[15] Zarrillo M, Miller H, Balasubramanian R, Wang H, Berg R, Eaton R, et al. Preliminary development of a real time seasonal load restriction system for remote sites. Cold Regions Engineering 2012: Sustainable Infrastructure Development in a Changing Cold Environment: ASCE 2012. p. 380–90.
[16] Marquis B. Mechanistic approach to determine spring load restrictions in Maine. Augusta, Maine: Maine. Dept. of Transportation; 2008.
[17] Marquis B. Mechanistic approach to determine spring load restrictions in Maine. Augusta, Maine: Maine. Dept. of Transportation; 2008. p. 1–25.
[18] Mahoney J, Rutherford M, Hicks R. Guidelines for spring highway use restrictions. Federal Highway Admin 1987:1–15.
[19] Kestler MA, Berg RL, Steinert BC, Hanek GL, Truebe MA, Humphrey DN. Determining when to place and remove spring load restrictions on low-volume roads: Three low-cost techniques. Transp Res Rec 2007;1989:219–29.
[20] Yesiller N, Benson CH, Bosscher PJ. Comparison of load restriction timings determined using FHWA guidelines and frost tubes. J Cold Reg Eng 1996;10:6–24.
[21] C-SHRP. Seasonal load restrictions in Canada and around the world. Canadian Strategic Highway Research Program; 2000. p. 1–8.
[22] Van Deusen D, Schrader C, Bullock D, Worel B. Springtime thaw weakening and load restrictions in Minnesota. Transport Res Record: J Transport Res Board 1998:21–8.
[23] Bradley A, Ahammed M, Hilderman S, Kass S. Responding to climate change with rational approaches for managing seasonal weight programs in Manitoba. Cold Regions Engineering 2012: Sustainable Infrastructure Development in a Changing Cold Environment; 2012. p. 391–401.
[24] Baïz S, Tighe S, Haas C, Mills B, Perchanok M. Development of frost and thaw depth predictors for decision making about variable load restrictions. Transport Res Record: J Transport Res Board 2008:1–8.
[25] Chapin J, Kjartanson BH, Pernia J. Comparison of two methods for applying spring load restrictions on low volume roads. Can J Civ Eng 2012;39:599–609.
[26] Jiji LM, Ganatos P. Approximate analytical solution for one-dimensional tissue freezing around cylindrical cryoprobes. Int J Therm Sci 2009;48:547–53.
[27] Bao T, Liu Z, Bland J. A multivariate freezing-thawing depth prediction model for spring load restriction. Cold Reg Sci Technol 2019;167. 102856.
[28] Konrad J-M. Physical processes during freeze-thaw cycles in clayey silts. Cold Reg Sci Technol 1989;16:291–303.
[29] Aldrich HPJ, Paynter HM. Analytical studies of freezing and thawing of soils. Boston, MA: Arctic Construction and Frost Effects Lab; 1953.
[30] Berg RL, Kestler MA, Eaton RA, Benda CC. Estimating when to apply and remove spring load restrictions. Current Practices in Cold Regions Engineering. Orono, Maine, USA: American Society of Civil Engineers; 2006. p. 1–11.
[31] Bertsekas DP. Constrained optimization and Lagrange multiplier methods. Academic Press; 2014.
[32] Gill PE, Wong E. Sequential quadratic programming methods. Mixed integer nonlinear programming. Springer; 2012. p. 147–224.
[33] McBane JA, Hanek G. Determination of the critical thaw-weakened period in asphalt pavement structures; 1986.